Journal of Materials Chemistry A

RSC Publishing

PAPER

View Article Online
View Journal | View Issue

Reduced TiO_2 nanotube arrays for photoelectrochemical water splitting†

Cite this: *J. Mater. Chem. A*, 2013, **1**, 5766

Qing Kang,[a] Junyu Cao,[b] Yuanjian Zhang,[a] Lequan Liu,[a] Hua Xu[abc] and Jinhua Ye*[abcd]

We report a facile one-step chemical method to synthesize partially reduced TiO_2 nanotube arrays (NTAs). The $NaBH_4$ treatment introduces oxygen vacancies on the surface and interior of TiO_2. Oxygen vacancy extends the photocatalytic activity of TiO_2 NTAs from the UV to visible light region, and enhances the electrical conductivity as well as charge transportation. Surface oxygen vacancies serve as charge carrier traps as well as adsorption sites where the charge transfer to adsorbed species inhibits the surface charge recombination, whereas bulk oxygen vacancies tend to act as charge carrier traps where e–h recombination occurs. The optimally reduced TiO_2 NTAs yield a photocurrent density of 0.73 mA cm^{-2} at 1.23 V_{RHE} and a highest photoconversion efficiency of 1.31% at a rather low bias of 0.40 V_{RHE} under a standard AM 1.5G solar illumination. Not only does the incident photon to current conversion efficiency (IPCE) spectrum increase in the UV region, but photoactivity in visible light also emerged. Surface oxygen vacancies, serving as electron donors, cause a noticeable negative flatband shift and increase the donor density of TiO_2 NTAs 2-fold. Electron paramagnetic resonance (EPR) spectra confirm the presence of oxygen vacancies on the surface and interior of TiO_2. Benefitting from the oxygen vacancy, a narrowed band gap of 2.46 eV and suitable localized states for hydrogen production are observed.

Received 15th February 2013
Accepted 5th March 2013

DOI: 10.1039/c3ta10689f

www.rsc.org/MaterialsA

Introduction

Ever since 1971, when Honda and Fujishima discovered the photooxidation of water on titanium dioxide (TiO_2),[1] the photoactivation of TiO_2 has been extensively investigated. To date, TiO_2 has been widely applied in photocatalysis for environmental cleanup, solar cells, clean H_2 energy production, antibacterial activity and more.[2] As one of the most studied photocatalyst materials, TiO_2 has many advantages: its abundance, low cost, low toxicity, superior photostability, and high intrinsic catalytic activity under UV illumination.[3] However, the solar to hydrogen efficiency of TiO_2 is substantially limited by its large band gap energy and electron–hole recombination.[4] An enormous amount of research has been focused on enhancing visible light absorption. Metallic and nonmetallic elements doping TiO_2 to generate donor or acceptor states in the band gap is a versatile approach to extend the optical absorption to the visible region.[5,6] However, problems such as increased carrier recombination centers and decreased incident photon to electron conversion efficiency (IPCE) in the UV light absorption region represent significant limitations for this strategy.[6] Thereby, to further improve the photoelectrochemical (PEC) activity of TiO_2 by a doping strategy, an important issue is to solve the diminution of IPCE in the UV region.

Oxygen vacancies (Ti^{3+}) are known to be shallow donors with relatively low formation energy.[7] It has been reported that oxygen vacancy plays a critical role in determining the surface and electronic properties of TiO_2.[8,9] Reduced TiO_2 (TiO_{2-x}), which contains Ti^{3+} or oxygen vacancy, has been demonstrated to exhibit visible light absorption.[10,11] The introduced oxygen vacancy creates localized states in the band gap,[8,10] which extends its optical absorption to the visible region. Nevertheless, the vacancy states localize at 0.75 to 1.18 eV below the conduction band minimum of rutile phase TiO_2 (−0.29 eV), which is lower than the redox potential for hydrogen evolution. Therefore, it is important to develop visible-light responsive TiO_2 with high performance for hydrogen production from water splitting. Moreover, the reported methods to produce reduced TiO_2 are mainly focus on hydrogenation methods, chemical vapor deposition, and high energy particle (laser, electron or Ar^+) bombardment.[12,13] However, these strategies need harsh synthesic conditions or expensive facilities which

[a]*International Center for Materials Nanoarchitectonics (WPI-MANA), National Institute for Materials Science (NIMS), 1-1 Namiki, Tsukuba, Ibaraki 305-0044, Japan. E-mail: Jinhua.YE@nims.go.jp*

[b]*Catalytic Materials Group, Research Unit for Environmental Remediation Materials, National Institute for Materials Science (NIMS), 1-1 Namiki, Tsukuba, Ibaraki 305-0044, Japan*

[c]*Graduate School of Chemical Science and Engineering, Hokkaido University, Sapporo, Japan*

[d]*TU-NIMS Joint Research Center, School of Materials Science and Engineering, Tianjin University, 92 Weijin Road, Nankai District, Tianjin 300072, P. R. China*

† Electronic supplementary information (ESI) available: OCP, XRD, TEM, XPS, and EPR. See DOI: 10.1039/c3ta10689f

limit their practical application. Furthermore, the surface Ti^{3+} is unstable in air or in electrolyte as it is easily oxidized by air or dissolved oxygen in water.[14–16] Zuo *et al.*[14] reported a combustion method to reduce Ti(IV) to Ti(III) by reducing gas (CO and NO). However, this inevitably introduces foreign species into the TiO_2 lattice. Hence, developing a simple and economical strategy to synthesize a stable reduced TiO_2 photocatalyst with suitable localized states is still a great challenge.

In addition to enhancing optical absorption, it is equally important to improve the morphology and electronic structure of TiO_2 for effective separation and transportation of photoexcited charge carriers. Vertically oriented TiO_2 nanotube arrays (NTAs) prepared on Ti foil by electrochemical anodization are considered to be a very effective structure for PEC water splitting.[17] The high surface area, high orientation, and uniform interfacial structure permit significant light absorption depths and enhance the charge separation by providing high electrode–electrolyte interface areas and shortening the minority charge carrier transport distance to the electrolyte.[17,18]

We hypothesize that reducing TiO_2 nanostructures in a reducing reagent will substantially increase the density of oxygen vacancies (donor density) and, thereby, enhance the electrical conductivity as well as charge transportation. To prove this hypothesis, we have focused on $NaBH_4$-treated nanotube arrays (denoted as reduced TiO_2 NTAs). $NaBH_4$, a common widely used reducing reagent was chosen because of its high reducing ability of reducing Ti(IV) to Ti(III). The reaction is as follows:

$$NaBH_4 + 8OH^- \rightarrow NaBO_2 + 8e^- + 6H_2O$$

$$Ti^{4+} + e^- \rightarrow Ti^{3+}$$

In comparison to previously widely adopted hydrogenation at high temperature, this chemical method can avoid the risk of explosion in the experimental procedure. In the present study, we report a facile one-step method to synthesize partially reduced TiO_2 NTAs at room temperature, which exhibit high activation for PEC water splitting. The increased surface oxygen vacancy (donor density) decreases the surface recombination centers, enhances the electrical conductivity, and improves the charge transportation. To our knowledge, this is the first simple chemical method to produce one-dimensional reduced TiO_2 nanostructures for PEC water splitting.

Experimental details

Fabrication of the reduced TiO_2 NTAs on Ti substrate

Before anodization, the titanium foils (Aldrich 0.25 mm, 99.7%) were ultrasonically cleaned in acetone and ethanol for 5 min each. The cleaned titanium foils were anodized at a constant potential of 80 V in an ethylene glycol solution containing 0.3 wt% NH_4F and 2 vol% H_2O at 5 °C for 30 min in a two-electrode configuration with a graphite cathode. After anodic oxidation, the samples were rinsed with ethanol and water and dried in air. The resulting amorphous titania nanotube arrays were annealed at 450 °C for 3 h with heating and cooling rates of 5 °C min^{-1} in air to crystallize the tube walls and improve their photocatalytic activity. Finally the annealed nanotube arrays were dipped in 0.1 M $NaBH_4$ for different times at room temperature followed by rinsing with water and air drying.

Characterization

The morphologies were studied using a JEOL JSM 6700F field-emission scanning electron microscope (FE-SEM). The phase of the samples was identified by an X-ray diffractometer (XRD, RINT 2000; Rigaku Corp.) employing Cu Kα radiation (λ = 1.54178 Å). UV-vis diffuse reflectance absorption spectra (DRS) were obtained on a UV-visible spectrophotometer (UV-2500PC; Shimadzu Corp.). Raman spectra were obtained on a laser Raman spectrometer (NRS-1000, Jasco Corp.) with a backscattering configuration using an Ar^+ laser (20 mW, 532 nm) as excitation source. Photoluminescence (PL) spectra were recorded using a Hitachi F-2500 fluorescence spectrophotometer at an excitation wavelength of 310 nm. X-ray Photoelectron Spectroscopy (XPS) experiments were performed in a Theta probe (Thermo Fisher) using monochromated Al Kα X-rays at $h\nu$ = 1486.6 eV. Peak positions were internally referenced to the C1s peak at 284.6 eV. The Electron Paramagnetic Resonance (EPR) of the samples was recorded to confirm the presence of high spin Ti^{3+} as well as oxygen vacancy on a JES-FA200 Electron Spin Resonance Spectrometer.

Photoelectrochemical activity measurement

PEC activity measurements were performed with a CHI electrochemical analyzer (ALS/CH model 650A) using a standard three-electrode mode with 1 M NaOH (pH = 13.9) solution as the electrolyte. The reduced TiO_2 NTA photoanodes were used as working electrodes; a Pt sheet served as counter-electrode. An Ag/AgCl (saturated KCl) electrode (RE-1C; BAS Inc.) was used as the reference electrode. A 500 W Xe lamp (Optical ModuleX; Ushio Inc.) was used as the solar light source, and the incident light intensity at 300–800 nm was measured to be 0.6 W cm^{-2} using a spectroradiometer (USR-40; Ushio Inc.). The simulated sunlight was obtained by an AM 1.5 solar simulation (WXS-80C-3 AM 1.5G) with a light intensity of 100 mW cm^{-2}. Linear sweep voltammetry (LSV) was performed with a voltage scan speed of 0.01 V s^{-1} and the light was chopped manually at regular intervals. The incident photon to electron conversion efficiency (IPCE) was calculated from chronoamperometry measurements using a motorized monochrometer (M10; Jasco Corp.). The measured potential *vs.* the Ag/AgCl were converted to the reversible hydrogen electrode (RHE) scale *via* the Nernst equation:

$$E_{RHE} = E_{Ag/AgCl} + 0.059\ pH + E^{o}_{Ag/AgCl}$$

where E_{RHE} is the converted potential *vs.* RHE, $E_{Ag/AgCl}$ is the experimental potential measured against Ag/AgCl reference electrode, and $E^{o}_{Ag/AgCl}$ = 0.1976 V at 25 °C. Electrochemical

impedance spectroscopy (EIS) was performed at similar conditions as described above for photoelectrochemical tests. The amplitude of the sinusoidal wave was 5 mV and the frequency range examined was 100 kHz to 1 Hz.

Photoelectrochemical water splitting

PEC water splitting was carried out in an Ar gas flow system. The amounts of evolved gases were determined by gas chromatography (Shimadzu, GC-8A, TCD, Ar carrier). The light source was a 300 W Xe-lamp (Hayashi Tokei, Luminar Ace 210). A cutoff filter of 420 nm was employed for the visible-light irradiation. The light intensity (0.37 W cm^{-2}) was measured by a spectroradiometer (Ushio, USR-40). The electrolytes were bubbled with N_2 or Ar before measurements to remove dissolved O_2.

Results and discussion

Morphology characterization

The FE-SEM image in Fig. 1A indicates that the TiO_2 NTAs have an average length of ~7 μm and inner pore diameter of approximately 100 nm. The presence of well-aligned NTs vertically oriented from the Ti foil substrate promotes directional charge transport due to the one-dimensional features of the tubes. Fig. 1B shows that the reduced TiO_2 NTAs after $NaBH_4$ treatment have kept their porous structure, indicating the $NaBH_4$ treatment has not destroyed the nanostructure of TiO_2 NTAs. Closer observation reveals that the reduced nanotubes in Fig. 1B clearly separate with each other and the wall gets thinner compared with the pristine nanotubes shown in Fig. 1A. This indicates that $NaBH_4$ has indeed reacted with TiO_2. According to a previous report, thinner walls benefit the charge transport in TiO_2 NTAs.[17,18] We can infer that the reduced TiO_2 NTAs promise a high photocatalytic activity.

Photoelectrochemical properties

We have studied the photocurrents of reduced TiO_2 NTA photoanodes as a function of $NaBH_4$ treatment time, and then compared them to that of the pristine TiO_2 NTAs. As shown in Fig. 2A, all of the reduced TiO_2 NTAs have higher photoactivity than the pristine TiO_2 NTAs. Significantly, a 3-fold enhanced photocurrent density for the 40 min $NaBH_4$ treated sample is observed. Fig. 2B shows that the photocurrent densities of reduced TiO_2 NTAs, obtained at a potential bias of 1.23 V_{RHE}, increase gradually with the increase of the $NaBH_4$ treatment time from 10 to 40 min. The 40 min treated sample yields a maximum photocurrent density of 5.64 mA cm^{-2} at 1.23 V_{RHE}. The photocurrent density of reduced TiO_2 NTAs decrease, as the $NaBH_4$ treatment time is further increased above 40 min. Photocatalysis or PEC reactions primarily take place on the catalyst surface. The reaction efficiencies and related mechanisms would be greatly determined by surface properties, such as surface oxygen vacancy. If the surface interfacial electron transfer rate and photocurrent is large, the PEC performance is high. It is reported that surface oxygen vacancies serve as charge carrier traps as well as adsorption sites where the charge transfer to adsorbed species can prevent e–h recombination, whereas bulk oxygen vacancies tend to act as charge carrier traps where e–h recombination occurs.[19] A longer $NaBH_4$ treatment would cause a high concentration of bulk oxygen vacancies in TiO_2 and result in a reduced photocatalytic efficiency. Similar results are obtained on surface fluorinated-TiO_2 nanoporous film.[20]

Fig. 3 shows that reduced TiO_2 NTAs present higher photocurrents than pristine TiO_2 NTAs. The photocurrent of 40 min reduced TiO_2 NTAs reaches 0.732 mA cm^{-2} at 1.23 V_{RHE}, while pristine TiO_2 NTAs only contribute 0.193 mA cm^{-2}. Moreover, the 60 min reduced TiO_2 NTAs show an obvious decay following the initial fast increase of currents, suggesting a classical onset of recombination,[21–23] while the pristine and short time reduced TiO_2 NTAs do not show this character, confirming that inner oxygen vacancies serve as charge carrier traps where the electron–hole recombination occurs.

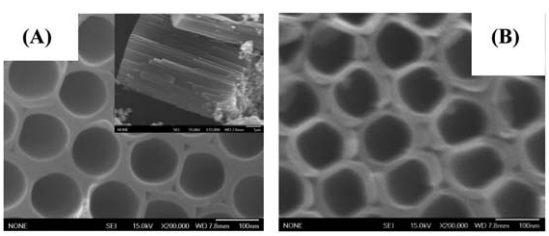

Fig. 1 SEM images of the TiO_2 NTAs before (A) and after (B) $NaBH_4$ treatment.

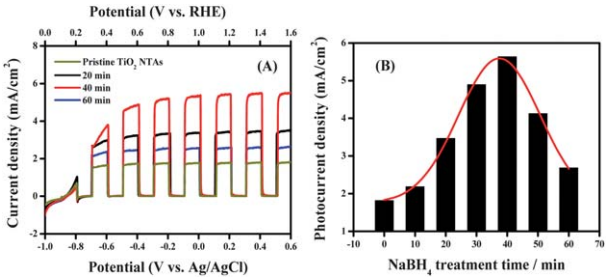

Fig. 2 (A) Linear sweep voltammetry (LSV, 10 mV s^{-1}) of the pristine and reduced TiO_2 NTAs measured in 1 M NaOH solution under UV-visible light irradiation (0.6 W cm^{-2}). (B) Measured photocurrent density of the reduced TiO_2 NTAs at 1.23 V_{RHE} as a function of $NaBH_4$ treatment time.

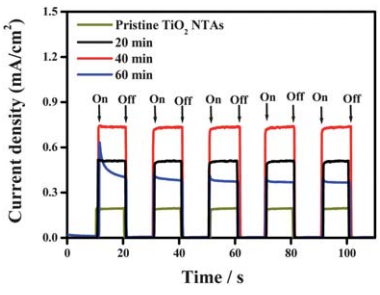

Fig. 3 Photocurrent density of the pristine and reduced TiO_2 NTAs at 1.23 V_{RHE} measured in 1 M NaOH solution under simulated solar light irradiation.

To investigate the effect of $NaBH_4$ treatment on the PEC performance of TiO_2 NTAs, Fig. 4A compares the linear sweeps of pristine and reduced TiO_2 NTAs prepared with different $NaBH_4$ treatment time, in a potential range of 0 to 1.6 V_{RHE}. As shown in Fig. 4A, upon illumination, the current gradually increases with increasing applied potential from 0 to 0.4 V_{RHE}, indicating photogenerated hole–electron separation resulting from the electric field.[24,25] At higher potentials ($E > 0.4$ V_{RHE}), a saturation of the photoresponse is observed for all the samples. Beranek *et al.*[26] ascribed this limit of photocurrent to the field distribution on the nanotubes. For a tube shaped n-type semiconductor, the majority carrier-depleted zones, the space-charge layers, are generated at both sides of the tube walls, while for compact layer film, the potential dependence is in line with the Gärtner model[27] predicting $I_{ph} \propto E^{0.5}$. In comparison to pristine TiO_2 NTAs, the reduced TiO_2 NTAs exhibit at least two times enhanced photocurrent over the entire potential window. It confirms that $NaBH_4$ treatment is an effective method for enhancing the PEC performance of TiO_2 NTAs. The onset potentials of all the reduced TiO_2 NTAs shift negatively compared with that of the pristine TiO_2 NTAs (from 0.16 V_{RHE} to 0.08 V_{RHE}). The shift in the onset potential might be due to either a lower band bending requirement for separating electrons and holes because of the material's likely possession of better charge–transport properties than pristine TiO_2, or faster surface kinetics as a result of $NaBH_4$ treatment.[28] The more negative onset potentials on reduced TiO_2 NTAs mean that the charge separation and transportation is more efficient. Fig. 4B is the corresponding light energy to chemical energy conversion (photoconversion) efficiency calculated using the following equation:[9,29,30]

$$\eta = I(1.23 - V)/J_{light}$$

where V is the applied bias *vs.* RHE, I is the photocurrent density at the measured bias, and J_{light} is the irradiance intensity of 100 mW cm^{-2} (AM 1.5G). The pristine TiO_2 sample exhibits an optimal conversion efficiency of 0.32% at 0.48 V_{RHE}. Significantly, the 40 min reduced TiO_2 NTAs achieve the highest efficiency of 1.31% at 0.40 V_{RHE}. Likewise, the 20 min and 60 min reduced TiO_2 NTAs exhibit the optimal efficiency of 0.85% and 0.57% at a similar applied bias. $NaBH_4$ treatment substantially enhances the photoconversion efficiency of TiO_2 NTAs by improving the maximum photocurrent and shifts the onset potential negatively.

To understand the interplay between the photoactivity and light absorption of reduced pristine TiO_2 NTAs, we have quantitatively investigated their photoactivity as a function of wavelength of incident light. In comparison to photocurrent density obtained under white light illumination, photocurrents as a function of the wavelength and incident photon to current conversion efficiency (IPCE) are much better parameters to characterize the photoconversion efficiency of different photoanodes because they are independent from the light sources and filters used in the measurement.[9,31] IPCE can be expressed by the following equation:[3,9]

$$\mathrm{IPCE}(\lambda) = 1240 j_p(\lambda)/\lambda E_\lambda(\lambda)$$

Where $j_p(\lambda)$ is the measured photocurrent density (mA cm^{-2}) and $E_\lambda(\lambda)$ is the incident light power density (mW cm^{-2}) for each wavelength, λ (nm). Fig. 5A shows the measured photocurrent of the pristine and reduced TiO_2 NTAs as a function of the wavelength and Fig. 5B contains the corresponding IPCE spectra. Fig. 5 shows that the reduced TiO_2 NTAs exhibit significantly enhanced photoactivity in the UV region. Particularly, the reduced TiO_2 NTAs have the highest IPCE values of 68.7% at 330 nm, which is 2 times higher than that of the pristine TiO_2 NTAs. It indicates that the UV light was effectively used for PEC water splitting, in which the separation and transportation of photoexcited charge carriers are very efficient in the reduced TiO_2 NTAs.[9] Significantly, the IPCE values show a small peak at 460 nm (Fig. 5B, inset). This is direct evidence for a visible light photoresponse of reduced TiO_2 NTAs. The enhanced visible light photoresponse is not at the expense of IPCE in UV region, which is not consistent with previous reports. These results described here confirm that the enhanced photocurrent in reduced TiO_2 NTAs is mainly attributed to the improved IPCE in the UV region, while the newly developed visible light absorption also made a partial contribution.

To gain more in-depth understanding of the charge–transport properties of reduced and pristine TiO_2 NTAs, we investigated the electron recombination kinetics of these two types of NTAs. The electron recombination kinetics was investigated by monitoring the transient V_{oc} as a function of time upon turning off the illumination. Under open-circuit conditions, electrons

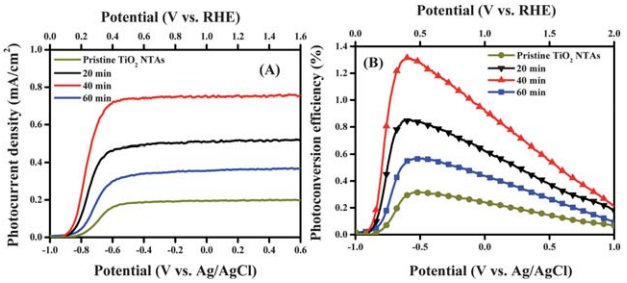

Fig. 4 (A) *I–V* plot collected from pristine and reduced TiO_2 NTAs. (B) The corresponding light energy to chemical energy conversion (photoconversion) efficiency.

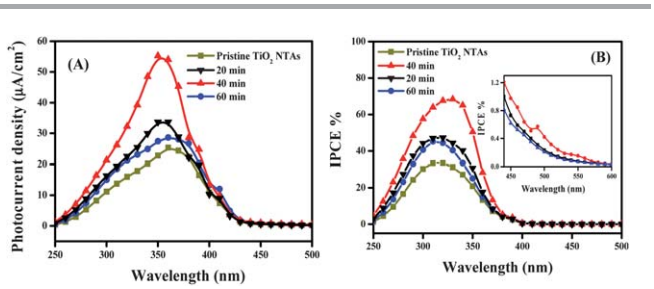

Fig. 5 (A) Measured photocurrent of the pristine and reduced TiO_2 NTAs as a function of the wavelength. (B) The corresponding IPCE spectra of the pristine and reduced TiO_2 NTAs.

accumulate within the nanostructure semiconductor films following solar light irradiation and shifting the apparent Fermi level to negative potentials. Once the illumination is stopped, the accumulated electrons are slowly discharged because they are scavenged by redox species in the electrolyte.[32] The electron density in the conduction band decays sharply due to charge recombination, with the V_{oc} decay rate directly determined by the recombination rate. Fig. 6A and Fig. S1† plot the V_{oc} decay as a function of time measured based on the pristine and reduced TiO_2 NTA anodes. It is evident that the reduced TiO_2 NTA anode has a significantly slower V_{oc} decay rate than that based on pristine TiO_2 NTAs, suggesting slow recombination kinetics in reduced TiO_2 NTAs. From the V_{oc} decay rate, the lifetime of photogenerated electrons (τ_n), the average time that the photogenerated electrons exist before they recombine, can be calculated by the following expression:[33–35]

$$\tau_n = -(k_B T/e)(dV_{oc}/dt)^{-1}$$

where k_B is Boltzmann's constant, T is temperature, and e is the elementary charge. The calculated τ_n is plotted in Fig. 6B as a function of V_{oc} for the two types of anodes. It is observed that τ_n of the reduced TiO_2 NTAs is longer than that of pristine TiO_2 NTAs. The extended τ_n observed in reduced TiO_2 NTAs compared to that observed in pristine TiO_2 NTAs may be attributed to the surface defects, which act as adsorption sites benefiting the charge carrier transportation.

EIS provides a powerful method for the study of charge transfer and recombined processes at semiconductor–electrolyte interfaces.[20,36,37] A typical Nyquist plot obtained at different potentials in 1.0 M NaOH aqueous solution for the illuminated pristine and reduced TiO_2 NTAs is shown in Fig. 7. After $NaBH_4$ treatment, the light EIS arc of the electrode becomes smaller at the same potential. According to previous results,[20,37] the smaller size of the semicircle arc diameter indicates a more effective separation of the photogenerated electron–hole pair and/or a faster interfacial charge transfer to the electron donor–acceptor.

Additionally, the flatband potential (E_{fb}) of the pristine and reduced TiO_2 NTAs was calculated using the following Mott–Schottky equation:[38,39]

$$1/C^2 = (2/e_0\varepsilon\varepsilon_0 N_d)(E_{app} - E_{fd} - KT/e_0)$$

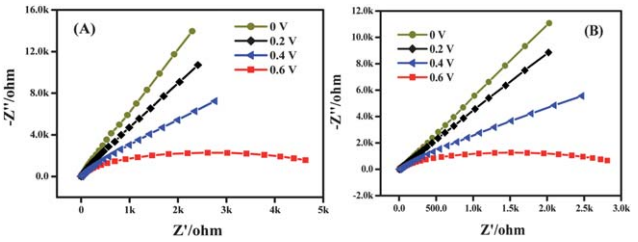

Fig. 7 EIS responses of pristine (A) and reduced (B) TiO_2 NTAs under different bias potentials *versus* Ag/AgCl in 1.0 M NaOH solutions with solar light illumination.

Here, C is the differential capacitance of the Helmholtz layer, e_0 is the electron charge, ε the dielectric constant of TiO_2 ($\varepsilon = 10$),[26] ε_0 the permittivity of vacuum, N_d the donor density, and E_{app} the applied bias at the electrode. Fig. 8A shows the Mott–Schottky plots for the pristine and reduced TiO_2 NTAs at a frequency of 1 kHz. The E_{fb} was estimated to be 0.45 and 0.38 V_{RHE} for pristine and reduced TiO_2 NTAs, respectively. The exceptionally low E_{fb} for reduced TiO_2 NTAs indicates a very efficient charge separation and transportation. The negative shift of E_{fb} upon $NaBH_4$ reduction is reported here for the first time in aqueous solution. In fact, Fig. 4A has shown indirect evidence for that. According to the well-known Gärtner equation, where only the recombination of photocarriers in bulk phase is considered,[39] the onset potential of photocurrent corresponds to the flatband potential. The donor density of the pristine and reduced TiO_2 NTAs was determined from the slope of the Mott–Schottky plots. All TiO_2 samples show a positive slope in the Mott–Schottky plots, as expected for n-type semiconductor (Fig. 8A). Importantly, the reduced TiO_2 NTAs show substantially smaller slopes of Mott–Schottky plot compared to the pristine TiO_2 sample, suggesting an increase of donor densities. The donor densities were calculated from the slopes of Mott–Schottky plots using the equation:

$$N_d = (2/e_0\varepsilon\varepsilon_0)[d(1/C^2)/dE_{app}]^{-1}$$

The calculated donor densities of the pristine and reduced TiO_2 NTAs are 8.93×10^{17} and 2.06×10^{18} cm^{-3}, respectively. $NaBH_4$ treatment increases the donor density of TiO_2 NTAs 2-fold, by creating surface oxygen vacancies that serves as electron

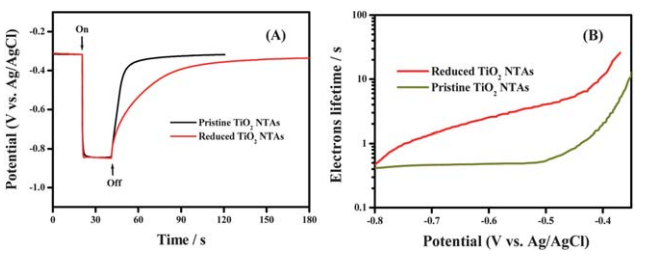

Fig. 6 (A) Open circuit potential of the pristine and reduced TiO_2 NTAs under simulated solar light irradiation. (B) The corresponding electron lifetimes as a function of open circuit potential.

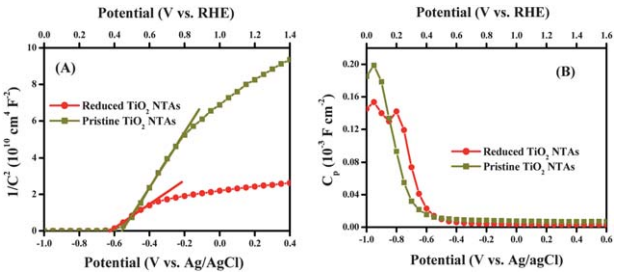

Fig. 8 (A) Mott–Schottky plots of the pristine and reduced TiO_2 NTAs collected at a frequency of 1 kHz. (B) Measured parallel capacitance (C_p) *versus* the applied potential plot at 50 Hz for the pristine and reduced TiO_2 NTAs.

donors.[7,9] The increased donor density enhances the electrical conductivity as well as charge transport in TiO_2. Moreover, the increased donor density is expected to shift the Fermi level of TiO_2 toward the conduction band.[8,9] The upward shift of the Fermi level facilitates the charge separation at the semiconductor–electrolyte interface, by increasing the degree of band bending at the TiO_2 surface.[9] The enhanced charge separation and transportation are the major reasons for the observed IPCE enhancement. Fig. 8B shows the parallel capacitance (C_p) plotted against the applied potential. As shown in Fig. 8B, one peak appears at 0.05 V_{RHE} for pristine TiO_2 NTAs. According to the previous conclusions, the different positions of the capacitance peak may involve diverse surface defects.[20] This indicates that there is only one kind of surface defect on the pristine TiO_2 NTAs, whereas for the reduced TiO_2, the peak density decreases and a new peak at 0.2 V_{RHE} emerges. This indicates that the reduction process decreases the original surface defects on TiO_2 and even possibly gave rise to new surface defects.

To guarantee that the obtained photocurrent is due to water splitting, it is important to determine the amounts of evolved H_2 and O_2 for PEC water splitting. Fig. 9 shows PEC water splitting using a reduced TiO_2 NTA film with 0.2 $V_{Ag/AgCl}$. The amount of H_2 evolved is similar to the half of the amount of electrons passing through the outer circuit. This result indicates that the observed photocurrent is due to water splitting. It should be noted that no other byproducts except H_2 and O_2 were detected by the gas chromatography, which means there is no other reaction happened during the water splitting.

Optical properties

Fig. 10 shows the UV-vis-NIR absorption spectra of the pristine and reduced TiO_2 NTAs. The pristine TiO_2 NTAs are only active under UV irradiation while the photoresponse of reduced TiO_2 NTAs is effectively extended into the visible and near infrared regions. It is reported that the visible and infrared absorption is positively related to oxygen vacancy in TiO_2. The inset shows that the band gap of the reduced and pristine TiO_2 NTAs, estimated from the main absorption edge of the profile, are about 2.99 and 3.09 eV, respectively. This decrease in the band gap is consistent with the assumption that an electronic band is located just below the conduction band of pure TiO_2.

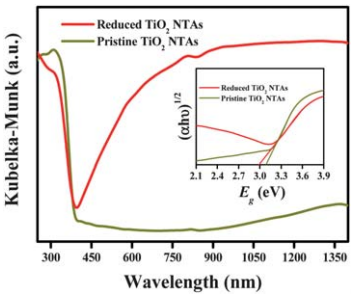

Fig. 10 UV-vis-NIR diffuse reflectance spectra of pristine and reduced TiO_2 NTAs.

We used Raman spectroscopy to examine surface structural changes in the TiO_2 nanocrystals after the introduction of oxygen vacancy by $NaBH_4$ treatment. The three polymorphs of TiO_2 belong to different space groups: D_{4h} (ref. 19) ($I4_1/amd$) for anatase, D_{2h} (ref. 15) ($pbca$) for brookite and D_{4h} (ref. 14) ($P4_2/mnm$) for rutile, which have distinctive characteristics in Raman spectra.[13] The pristine TiO_2 NTAs display three anatase Raman bonds at 396.9, 511.4 and 634.8 cm^{-1}, whereas new small bands at 244.9 and 322.0 cm^{-1} emerge for the reduced TiO_2 NTAs (Fig. 11). These two new Raman bands cannot be assigned to any of the three polymorphs of TiO_2, which indicates that surface structural changes occur after $NaBH_4$ treatment.

The PL spectra of anatase TiO_2 materials are mainly attributed to three kinds of physical origins: self-trapped exciton, oxygen vacancy, and surface defect.[40,41] Clearly, in comparison to the pristine TiO_2 NTAs, the reduced TiO_2 NTAs show four new bands at 420.4, 449.2, 464.4 and 495.0 nm (Fig. 12). The first two new bands are ascribed to surface defects and the latter two bands are associated with the oxygen vacancies forming at the surface of TiO_2 NTAs.[42,43] The emergence of surface oxygen vacancies is also supported by the results of C_p as discussed above. The proposed new surface oxygen vacancies and/or the shift in the positions of surface oxygen vacancies may act as the radiate recombination sites.

We examined the change of surface chemical bonding of TiO_2 nanocrystals induced by $NaBH_4$ treatment with XPS. Oxygen 1s XPS profiles shown in Fig. 13A are slightly shifted to lower energy after reduction process. The shift is in line with the transfer of electrons to the neighboring oxygen vacancies. We also observed a similar shift for Ti2p, as shown in Fig. 13B. This might suggest migration of electrons bound to oxygen

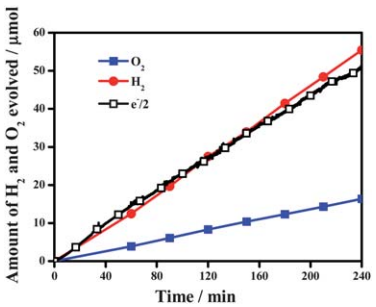

Fig. 9 PEC water splitting over reduced TiO_2 NTA film electrode under visible light irradiation (0.37 W cm^{-2}).

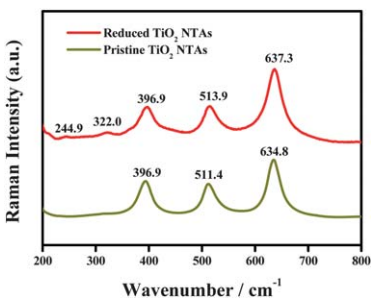

Fig. 11 Raman spectra of pristine and reduced TiO_2 NTAs.

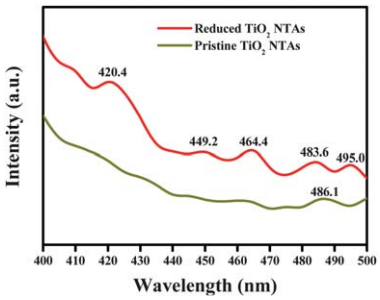

Fig. 12 Photoluminescence (PL) spectra of pristine and reduced TiO_2 NTAs (E_x: 310 nm).

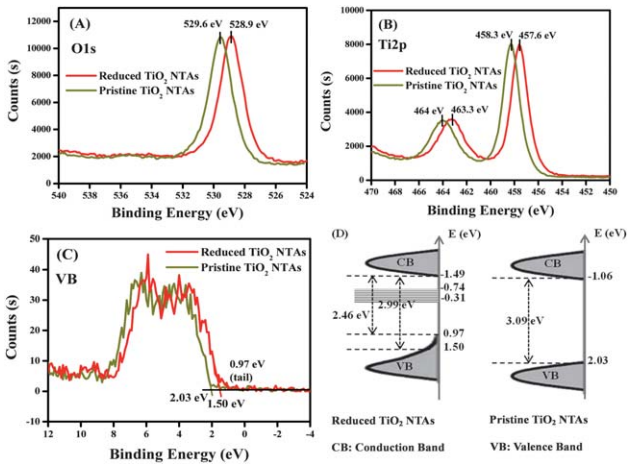

Fig. 13 (A) O1s (B) Ti2p (C) valence-band XPS spectra of the pristine and reduced TiO_2 NTAs. (D) Schematic illustration of the DOS of reduced TiO_2 NTAs, as compared to that of pristine TiO_2 NTAs.

and titanium ions towards oxygen vacancies, the latter serving as electron traps.[44–46] The density of states (DOS) of the valence band (VB) of TiO_2 nanocrystals was also measured by valence band XPS (Fig. 13C). The pristine TiO_2 NTAs displayed typical valence band DOS characteristics of TiO_2, with the edge of the maximum energy at ~2.03 eV below the Fermi energy. Since the optical band gap of pristine TiO_2 NTAs is 3.09 eV (Fig. 10 inset), the conduction band (CB) minimum would occur at −1.06 eV. On the other hand, the VB maximum energy of reduced TiO_2 NTAs showed notable blue-shift to ~1.50 eV and was followed by a band tail further toward ~0.97 eV. Combined with the results from optical measurements that suggest a narrowed band gap, the CB minimum of the reduced TiO_2 NTAs would occur at −1.49 eV. A schematic illustration of the DOS of reduced and pristine TiO_2 NTAs is shown in Fig. 13D. Chen *et al.* reported that the surface disorder induces a substantial shift (2.18 eV) of the VB position for hydrogenated black TiO_2 NPs,[13] while Naldoni *et al.*[47] recently prepared TiO_2 NPs with crystalline and defective cores and disordered shells, which induces a remarkable band gap narrowing (1.85 eV). In our case, $NaBH_4$ treatment is an effective method to introduce surface defect (oxygen vacancy) into TiO_2 NTAs. The surface defect induces a band gap narrowing (2.46 eV) based on the already predicted slight VB tailing. Furthermore, oxygen vacancy introduce localized states at 0.75–1.18 eV below the CB minimum of TiO_2.[8,10] Electronic transitions from both tailed VB and oxygen vacancy localized states are responsible for the reduced TiO_2 vis-NIR absorption. The energy positions of localized states are calculated as −0.74 to −0.31 eV, which contributed to the high performance for hydrogen production from water splitting.

To test for the presence of Ti^{3+}, low temperature EPR spectra are recorded in Fig. 14. The reduced TiO_2 NTAs give rise to a very strong EPR signal, while no signal is seen for the pristine TiO_2 NTAs. In the EPR spectra of reduced TiO_2 NTAs, there are three features: signals from electrons (Ti^{3+}), holes and O_2^-, which are labeled as signals A, B and C, respectively. The sharp signal at $g \approx 1.985$ is assigned to surface electron trapping sites in anatase TiO_2,[14,48] and is represented as signal A. The EPR signal with g value of 2.002 is due to surface hole trapping sites[48] and is represented as signal B. The surface Ti^{3+} would tend to adsorb atmospheric O_2, which could be reduced to O_2^- and shows EPR signal C at g-value of ~2.03.[49] Significant increases in signal A, B are obtained by increasing the $NaBH_4$ treatment time from 20 min to 40 min. On further increase of the $NaBH_4$ treatment time to 60 min, signals A and B decrease and signal C increases sharply, which means large amounts of surface Ti^{3+} are oxidized by adsorbed O_2. Among the three reduced TiO_2 NTAs, the 40 min sample shows the highest ratio of surface Ti^{3+} signal to superoxide (O_2^-) radical signal. This phenomenon indicates that $NaBH_4$ treatment for short time reduces surface TiO_2 into Ti^{3+} (oxygen vacancy). However, extended treatment will cause oxidation of surface oxygen vacancies. More surface oxygen vacancy results in better photoactivity. This is the reason that 40 min sample shows the highest photoactivity performance.

Stability and reproducibility

To test the stability of the samples, long time solar light illumination was performed. After 1 hour of solar light (AM 1.5G) illumination, the reduced TiO_2 NTAs retain their 90% photocurrent. Stored in air for one month, the sample still retained 80% of its initial visible light absorbance response. The reproducibility was tested on five samples; the inter-assay relative standard deviation is 1.82%. These results indicate good stability and excellent reproducibility of the sample.

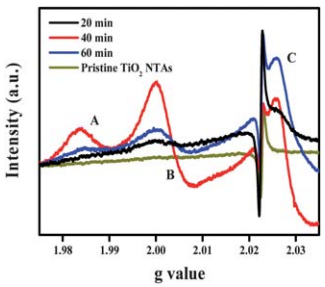

Fig. 14 EPR spectra for pristine and reduced TiO_2 NTAs.

Conclusions

Through a simple one-step chemical method partially reduced TiO_2 NTAs can be prepared. The PEC activity of the reduced TiO_2 NTAs is dependent on the $NaBH_4$ treatment time. The TiO_2 NTAs with a partially reduced surface exhibit enhanced visible light absorption and increased IPCE in the UV and visible regions. $NaBH_4$ treatment increases the donor density of TiO_2 NTAs 2-fold, by creating surface oxygen vacancies that serves as electron donors. The introduced surface oxygen vacancies account for the negative-shifted flatband potential; decreased surface recombination centers and favorable charge transfer rate. Benefitting from the oxygen vacancy, a narrowed band gap of 2.46 eV and suitable localized states for hydrogen production are observed. The present study sheds light on the importance of surface oxygen vacancy for narrowing the band gap and for the development of a highly active photocatalyst under visible light irradiation.

Acknowledgements

This work was partially supported by the World Premier International Research Center Initiative on Materials Nanoarchitectonics, MEXT, Japan. The authors thank Kiyotaka Iiyama for help with EPR measurements.

Notes and references

1 A. Fujishima and K. Honda, *Bull. Chem. Soc. Jpn.*, 1971, **44**, 1148–1150.
2 X. B. Chen and S. S. Mao, *Chem. Rev.*, 2007, **107**, 2891–2959.
3 T. Bak, J. Nowotny, M. Rekas and C. Sorrell, *Int. J. Hydrogen Energy*, 2002, **27**, 991–1022.
4 M. G. Walter, E. L. Warren, J. R. McKone, S. W. Boettcher, Q. Mi, E. A. Santori and N. S. Lewis, *Chem. Rev.*, 2010, **110**, 6446–6473.
5 X. B. Chen, S. H. Shen, L. J. Guo and S. S. Mao, *Chem. Rev.*, 2010, **110**, 6503–6570.
6 R. Asahi, T. Morikawa, T. Ohwaki, K. Aoki and Y. Taga, *Science*, 2001, **293**, 269–271.
7 A. Janotti, J. Varley, P. Rinke, N. Umezawa, G. Kresse and C. Van de Walle, *Phys. Rev. B: Condens. Matter Mater. Phys.*, 2010, **81**, 085212.
8 D. Cronemeyer, *Phys. Rev.*, 1959, **113**, 1222–1226.
9 G. Wang, H. Wang, Y. Ling, Y. Tang, X. Yang, R. C. Fitzmorris, C. Wang, J. Z. Zhang and Y. Li, *Nano Lett.*, 2011, **11**, 3026–3033.
10 I. Justicia, P. Ordejón, G. Canto, J. L. Mozos, J. Fraxedas, G. A. Battiston, R. Gerbasi and A. Figueras, *Adv. Mater.*, 2002, **14**, 1399–1402.
11 R. Sasikala, V. Sudarsan, C. Sudakar, R. Naik, L. Panicker and S. Bharadwaj, *Int. J. Hydrogen Energy*, 2009, **34**, 6105–6113.
12 T. L. Thompson and J. T. Yates Jr, *Chem. Rev.*, 2006, **106**, 4428–4453.
13 X. Chen, L. Liu, P. Y. Yu and S. S. Mao, *Science*, 2011, **331**, 746–750.
14 F. Zuo, L. Wang, T. Wu, Z. Zhang, D. Borchardt and P. Feng, *J. Am. Chem. Soc.*, 2010, **132**, 11856–11857.
15 K. Komaguchi, T. Maruoka, H. Nakano, I. Imae, Y. Ooyama and Y. Harima, *J. Phys. Chem. C*, 2010, **114**, 1240–1245.
16 A. Teleki and S. E. Pratsinis, *Phys. Chem. Chem. Phys.*, 2009, **11**, 3742–3747.
17 C. Grimes and G. K. Mor, *TiO_2 Nanotube Arrays: Synthesis, Properties, and Applications*, Springer Verlag, 2009.
18 C. A. Grimes, O. K. Varghese and S. Ranjan, *Light, water, hydrogen: the solar generation of hydrogen by water photoelectrolysis*, Springer Verlag, 2008.
19 M. Kong, Y. Li, X. Chen, T. Tian, P. Fang, F. Zheng and X. Zhao, *J. Am. Chem. Soc.*, 2011, **133**, 16414–16417.
20 X. Cheng, W. Leng, D. Liu, Y. Xu, J. Zhang and C. Cao, *J. Phys. Chem. C*, 2008, **112**, 8725–8734.
21 X. Cui, M. Ma, W. Zhang, Y. Yang and Z. Zhang, *Electrochem. Commun.*, 2008, **10**, 367–371.
22 A. Ghicov, B. Schmidt, J. Kunze and P. Schmuki, *Chem. Phys. Lett.*, 2007, **433**, 323–326.
23 H. Tsuchiya, J. M. Macak, A. Ghicov, A. S. Rader, L. Taveira and P. Schmuki, *Corros. Sci.*, 2007, **49**, 203–210.
24 N. K. Allam, K. Shankar and C. A. Grimes, *J. Mater. Chem.*, 2008, **18**, 2341–2348.
25 F. Y. Oliva, L. B. Avalle, E. Santos and O. R. Cámara, *J. Photochem. Photobiol., A*, 2002, **146**, 175–188.
26 R. Beranek, H. Tsuchiya, T. Sugishima, J. Macak, L. Taveira, S. Fujimoto, H. Kisch and P. Schmuki, *Appl. Phys. Lett.*, 2005, **87**, 243114.
27 W. W. Gärtner, *Phys. Rev.*, 1959, **116**, 84–87.
28 S. Hoang, S. Guo, N. T. Hahn, A. J. Bard and C. B. Mullins, *Nano Lett.*, 2012, **12**, 26–32.
29 M. G. Walter, E. L. Warren, J. R. McKone, S. W. Boettcher, Q. Mi, E. A. Santori and N. S. Lewis, *Chem. Rev.*, 2010, **110**, 6446–6448.
30 Q. X. Jia, K. Iwashina and A. Kudo, *Proc. Natl. Acad. Sci. U. S. A.*, 2012, **109**, 11564–11569.
31 A. Murphy, P. Barnes, L. Randeniya, I. Plumb, I. Grey, M. Horne and J. Glasscock, *Int. J. Hydrogen Energy*, 2006, **31**, 1999–2017.
32 A. Kongkanand, K. Tvrdy, K. Takechi, M. Kuno and P. V. Kamat, *J. Am. Chem. Soc.*, 2008, **130**, 4007–4015.
33 H. Yang, W. Fan, A. Vaneski, A. S. Susha, W. Y. Teoh and A. L. Rogach, *Adv. Funct. Mater.*, 2012, **22**, 2876.
34 J. H. Bang and P. V. Kamat, *Adv. Funct. Mater.*, 2010, **20**, 1970–1976.
35 A. Zaban, M. Greenshtein and J. Bisquert, *ChemPhysChem*, 2003, **4**, 859–864.
36 F. Fabregat-Santiago, G. Garcia-Belmonte, J. Bisquert, A. Zaban and P. Salvador, *J. Phys. Chem. B*, 2002, **106**, 334–339.
37 W. Leng, Z. Zhang, J. Zhang and C. Cao, *J. Phys. Chem. B*, 2005, **109**, 15008–15023.
38 A. Wolcott, W. A. Smith, T. R. Kuykendall, Y. Zhao and J. Z. Zhang, *Small*, 2009, **5**, 104–111.
39 L. Kavan, M. Grätzel, S. Gilbert, C. Klemenz and H. Scheel, *J. Am. Chem. Soc.*, 1996, **118**, 6716–6723.
40 X. Li, Y. Hou, Q. Zhao and G. Chen, *Langmuir*, 2011, **27**, 3113–3120.

41 A. K. L. Sajjad, S. Shamaila, B. Tian, F. Chen and J. Zhang, *Appl. Catal., B*, 2009, **91**, 397–405.
42 T. Tachikawa and T. Majima, *J. Am. Chem. Soc.*, 2009, **131**, 8485–8495.
43 N. Serpone, D. Lawless and R. Khairutdinov, *J. Phys. Chem.*, 1995, **99**, 16646–16654.
44 M. Senna, V. Sepelak, J. M. Shi, B. Bauer, A. Feldhoff, V. Laporte and K. D. Becker, *J. Solid State Chem.*, 2012, **187**, 51–57.
45 A. C. Papageorgiou, N. S. Beglitis, C. L. Pang, G. Teobaldi, G. Cabailh, Q. Chen, A. J. Fisher, W. A. Hofer and G. Thornton, *Proc. Natl. Acad. Sci. U. S. A.*, 2010, **107**, 2391–2396.
46 M. A. Henderson, W. S. Epling, C. H. F. Peden and C. L. Perkins, *J. Phys. Chem. B*, 2003, **107**, 534–545.
47 A. Naldoni, M. Allieta, S. Santangelo, M. Marelli, F. Fabbri, S. Cappelli, C. L. Bianchi, R. Psaro and V. Dal Santo, *J. Am. Chem. Soc.*, 2012, **134**, 7600–7603.
48 C. P. Kumar, N. O. Gopal, T. C. Wang, M. S. Wong and S. C. Ke, *J. Phys. Chem. B*, 2006, **110**, 5223–5229.
49 M. Anpo, M. Che, B. Fubini, E. Garrone, E. Giamello and M. C. Paganini, *Top. Catal.*, 1999, **8**, 189–198.

